European Polymer Journal 70 (2015) 342–359

Contents lists available at ScienceDirect

European Polymer Journal

journal homepage: www.elsevier.com/locate/europolj

Macromolecular Nanotechnology

Effects of surface modification and thermal annealing on the interfacial dynamics in *core–shell* nanocomposites based on silica and adsorbed PDMS

Panagiotis Klonos *, Apostolos Kyritsis, Polycarpos Pissis

Department of Physics, National Technical University of Athens, Zografou Campus, 15780 Athens, Greece

ARTICLE INFO

Article history:
Received 14 May 2015
Received in revised form 16 July 2015
Accepted 20 July 2015
Available online 21 July 2015

Keywords:
Silica polydimethylsiloxane composites
Core–shell
Rigid amorphous fraction
Interfacial dynamics
Dielectric spectroscopy

ABSTRACT

Core–shell structured nanocomposites of polydimethylsiloxane (PDMS) adsorbed onto high specific surface area (342 m^2/g) fumed silica nanoparticles (initially ~8 nm in size) were studied employing differential scanning calorimetry (DSC) and broadband dielectric spectroscopy (BDS). PDMS was adsorbed mainly onto the surfaces and voids of silica aggregates (~300 nm). Nanozirconia grafting on initial silica resulted in smoothening of external surfaces and in weaker polymer adsorption. The latter could be monitored by BDS via recording directly the relaxation mechanism (α_{int}) of polymer at the silica–PDMS interface. Surface modification led to suppression of interfacial dynamics (slower and weaker α_{int}). Spatial constraints (e.g. in voids and between crystal regions) were found to dominate mobility not close to the interfaces. In addition, thermal annealing of samples of enhanced interfacial mobility (unmodified surfaces) resulted in the suppression of α_{int}, similarly to the results of surface modification. In agreement to previous findings on similar systems, the characteristics of interfacial dynamics could be interpreted in terms of density of polymer–silica contact points at the interfaces (reduced for modified surfaces), in combination with models which involve bimodal conformations of polymer chains (loop- and tail-like) adsorbed on solid surfaces.

1. Introduction

Polymer nanocomposites [1] are well known systems which combine, in general, mild processing and improved physical properties, as compared to their initial components and conventional composites [2]. Due to the low volume of each nanoparticle the polymer may potentially interact with the filler at higher surface areas in nanocomposites, as compared to macroscopic particles at the same loadings in conventional composites [2]. Thus, the most widely adopted concept for rationalizing improvements of materials properties involves the existence of a fraction of polymer at interfaces between particles and polymer, characterized by modified structure [3–7], dynamics [8–11] and thermal stability [12,13], as compared to the bulk. The properties of interfacial polymer may affect significantly or even dominate the behavior of the whole system [14]. Kumar and coworkers have demonstrated that the interfacial layer thickness in the case of strongly adsorbing polymers may increase with particle size [15] and decrease with curvature of the nanoparticles (Ref. 7 in [15]). In general, the polymer in the interfacial layer is thought completely immobile, as it does not demonstrate any additive contribution to segmental

* Corresponding author.
E-mail address: pklonos@central.ntua.gr (P. Klonos).

http://dx.doi.org/10.1016/j.eurpolymj.2015.07.038
0014-3057/

mobility (e.g. to glass transition). On the other hand, Pissis and coworkers have suggested that the interfacial polymer is not completely immobile, since it demonstrates retarded dynamics, as recorded via an additional relaxation process, as compared to the bulk [8,9,16,17]. Moreover, they proposed that the increased interfacial layer thickness in polydimethylsiloxane(PDMS)/titania as compared to PDMS/silica nanocomposites [8,9,18] originates from the stronger particle–polymer hydrogen bonding. Furthermore, we have recently demonstrated that the structure of adsorbed complexes of linear PDMS onto high specific surface area fumed silica particles (aerosils) depends strongly on the adsorption conditions and the subsequent thermal treatment [17], similarly to polymers adsorbed on solid surfaces [19–21].

Parallel to the study of the interfacial layer in polymer nanocomposites, various studies of polymers adsorbed thermally or/and chemically on solid surfaces [19,20,22,23], as well as of thin polymer films [24], have demonstrated similarities between polymer nanocomposites and thin polymer films in thermal stability, polymer chain conformations and dynamics. *Core–shell* based nanocomposites [25,26] form a next class of interest in the same direction, where the polymer is adsorbed in multiple layers (*shells*) onto the nanoparticles (*core*). By controlling the amount of polymer adsorbed, next to the size of nanoparticles and the strength of polymer–particle interaction, the interfacial polymer fraction can be easily varied over wide ranges, practically up to 100% of the total polymer fraction. Thus, core–shell systems offer additional advantages for in–depth study of the interfacial polymer [11,17,27,28].

Computer simulations in polymers adsorbed on solid surfaces [7,29,30] have predicted increased density of the interfacial polymer, accompanied by slower dynamics, as compared to the bulk. The prolonged relaxation time of polymer in the surface region originates from the strong segment-surface attraction [29]. However, Borodin et al. [30] demonstrated that slower dynamics of poly(ethylene oxide) (PEO) at the interface with TiO_2 is better determined by the surface structure and electrostatic PEO–TiO_2 interactions, rather than the increased interfacial polymer density. Adoption of various conformations by polymer chains (tails, loops, trains [31]) at the interfaces with solid surfaces were found also of importance for predicting interfacial polymer properties [3,32–34]. Theodorou and coworkers [3,29] showed that polymer chains close to an attractive solid surface are pronouncedly flattened, or else more parallel to the surface, as compared to those away from the surface, this result coming in agreement with respective experimental studies [20,35]. Finally, Bitsanis and Brinke [32] and Harmandaris and coworkers [3,33,34] pointed to the polymer chain length as a crucial parameter for adoption of different conformations of polymers adsorbed on solid surfaces and of polymer confined between solid surfaces, respectively.

In the present work we study the dynamics and evaluate the fractions of interfacial polymer (polymer in the interfacial layer in close proximity to a solid surface) and of bulk and bulk-like polymer, all coexisting in the same silica/PDMS systems. Materials under investigation consist of linear polydimethylsiloxane (PDMS) adsorbed in amorphous fumed silica (SiO_2) aggregates, in systems of the *core–shell* type [36]. The adsorption is thought mainly physical (hydrogen bonding) [37]. In our 2 recent publications [17,27] on PDMS adsorbed on the same and similar initial (unmodified) silica [17], results have indicated that during the first stages of polymer adsorption (low polymer loading) PDMS adsorbed on the external surfaces of silica aggregates (high roughness) was ruled by slower dynamics (interfacial, α_{int} relaxation), as compared to the bulk (α relaxation, i.e. the fastest segmental relaxation which represents the unaffected amorphous polymer mobility). In the case of nanocomposites the segmental mobility of the polymer not close to the interface was observed only in samples of high PDMS loading, demonstrating however slower dynamics (α_c relaxation, bulk-like dynamics) as compared to the bulk (α), affiliated to spatial constraints in the voids of silica aggregates [17]. Additionally, we showed [27] that zirconia modification on fumed silica of low specific surface area, S_{BET}, (~58 m^2/g) resulted in slightly increased S_{BET} and in faster, stronger and more cooperative interfacial relaxation. In order to study in more depth the above effects, we manipulate here the surface characteristics of the initial silica of high S_{BET} (~342 m^2/g) by generating crystalline zirconia nanoparticles (same as in our recent study [27]) on the initial silica particles (smoothened surfaces), before adsorption of the polymer [36]. The investigation involves differential scanning calorimetry (DSC) for thermal transitions and broadband dielectric spectroscopy (BDS) for polymer dynamics. In addition to severe restriction of polymer crystallization, the results reveal significant effects of the silica particles on the segmental dynamics (related to glass transition), originating mainly from the strong reduction of molecular mobility at the interfaces. Surface effects were further studied by employing different thermal treatments (annealing of crystallization), which had been proved quite revealing in our previous study on similar core–shell based nanocomposites [17].

2. Experimental

2.1. Materials and code names

Preparation and morphological characterization of initial oxides have been previously described [36], therefore we repeat here briefly the preparation procedure. Fumed silica A-380 (pilot plant of the Institute of Surface Chemistry, Kalush, Ukraine) was used as initial substrate for the development of zirconia nanoparticles at various amounts by reiteration of the respective reaction cycle from 1 to 4 (resulted in ~6 and ~16 wt% zirconia, respectively [36]). Linear polydimethylsiloxane (Kremniypolymer, Zaporozhye, Ukraine, *MW* ~7960, degree of polymerization 105, viscosity ~1000 cPS) was adsorbed onto dry silica and modified silica at the amounts of 40 and 80 wt% from a hexane solution of PDMS (1 wt% PDMS). The suspensions were mechanically stirred and finally dried to remove solvents. Samples at PDMS content of 40 wt% are in the form of powder similar to initial A-380 powder, while at higher PDMS contents of 80 wt% and 100 wt%, the samples are liquid-like and liquid, respectively. In the finally produced materials silica (primary particle size ~8 nm) was found to form aggregates,

varying in size between 100 and 500 nm as observed previously by SEM [17]. Materials prepared and studied here and the specific surface modification by zirconia are interesting also in the perspective of biomedical applications, on the basis of biocompatibility of the components and control of hydrophilicity of initial silica [38,39].

Seven polymer nanocomposite compositions were prepared and studied in the present work, i.e. the initial PDMS, silica/PDMS with 40 and 80 wt% PDMS, and silica/zirconia/PDMS containing silica modified with 1 and 4 cycles of zirconia, again with 40 and 80 wt% PDMS. Throughout the text and in the figures and tables, representative code names that describe the samples are used. For instance (i) A380P80 corresponds to the sample in which PDMS at 80 wt% is adsorbed onto initial unmodified A-380, (ii) A380Z1P40 corresponds to the sample in which PDMS at 40 wt% is adsorbed onto A-380 that previously suffered 1 cycle of zirconia reaction, and (iii) A380Z4P80 corresponds to the sample in which PDMS at 80 wt% is adsorbed onto A-380 that previously suffered 4 cycles of zirconia reaction.

2.2. Differential scanning calorimetry (DSC)

Thermal transitions of the materials were investigated in helium atmosphere in the temperature range from −180 to 40 °C using a TA Q200 series DSC instrument, calibrated with Indium (for temperature and enthalpy) and Sapphires (for heat capacity). Samples of ~8 mg in mass were closed in standard Tzero aluminum pans (for powders) and Tzero hermetic aluminum pans (for liquids). Cooling and heating rates were fixed to 10 K/min for typical measurements (*Protocol A*). PDMS crystals melt at subzero temperatures, so a first heating scan for erasing thermal history was not necessary here. In order to enhance crystallization (during cooling), suppressed due to the presence of nanoparticles [9,17,40], measurements were carried out also after a 20 min isothermal stay (annealing) of the sample at a temperature between the onset and the peak (T_c) temperature of crystallization (*Protocol AC*). This annealing procedure resulted in maximum and stabilized degree of crystallinity, X_c. Finally, for initial PDMS we also performed fast cooling measurements (at ~90 K/min on average over the temperature region of crystallization, i.e. *quenching*) in order to evaluate the change in heat capacity at glass transition of the fully amorphous neat polymer during subsequent heating at 10 K/min.

Using the measured enthalpy of crystallization, $\Delta H_{c,DSC}$, and normalizing to the same polymer content, X_{PDMS}, according to Eq. (1)

$$\Delta H_{c,n} = \Delta H_{c,DSC}/X_{PDMS} \tag{1}$$

we have calculated the degree of crystallinity X_c employing Eq. (2),

$$X_c = \Delta H_{c,n}/\Delta H_{100\%} \tag{2}$$

in which $\Delta H_{100\%}$ is the enthalpy of fusion of fully crystallized PDMS, taken as 37.43 J/g [41].

As far as glass transition is concerned, the characteristic temperature T_g was determined as the midpoint of the heat capacity step during the transition. As in previous works [8,18], changes of ΔC_p between the neat polymer and nanocomposites based on the same polymer should be quantitatively compared, after the measured ΔC_p^{DSC} has been normalized to the same amorphous (not crystallized) polymer content, i.e. $X_{PDMS}(1 - X_c)$. Therefore, we normalized our results according to Eq. (3)

$$\Delta C_{p,n} = \frac{\Delta C_p^{DSC}}{X_{PDMS}(1 - X_c)} \tag{3}$$

2.3. Broadband dielectric spectroscopy (BDS)

Broadband dielectric spectroscopy (BDS) [42] measurements were carried out on samples of ~1 mm thickness for powders (compressed pellets, using a Perkin Elmer manual hydraulic press operating at ~10 tons) and ~50 μm thickness for liquids (employing thin silica spacers, to keep distance between the brass electrodes constant and ensure good electrical contacts). Samples were equilibrated under ambient conditions before measurements. Each sample was inserted between finely polished brass plates of a capacitor. This sandwich-like capacitor was inserted between the parallel electrodes of a Novocontrol BDS1200 sample cell and was mechanically griped in the mounting mechanism of the cell by hand force. Then, an alternate voltage was applied and the complex dielectric permittivity, $\varepsilon^* = \varepsilon' - i\varepsilon''$, was recorded isothermally (in nitrogen atmosphere) as a function of frequency in the range from 10^{-1} to 10^6 Hz at temperatures from −150 to 60 °C, on heating in steps of 2.5, 5 and 10 K (depending on the process under investigation) using a Novocontrol Alpha analyzer. The temperature was controlled to better than 0.5 K with a Novocontrol Quatro cryosystem. Again, this measurement protocol will be referred to as *Protocol A*. In order to investigate effects of crystallinity on the segmental dynamics, measurements were carried out also following the *Protocol AC*, i.e. after a 20 min isothermal stay (annealing) of the sample at a temperature between the onset and the peak of crystallization, as it was defined from DSC measurements. The sample was cooled down to −150 °C and the isothermal steps started. This annealing procedure led to a maximum degree of crystallinity, X_c, and, thus, no further changes of crystallinity during the subsequent measurements were observed. BDS measurements were carried out also isochronally at 125 Hz during heating in the temperature range between −150 and 60 °C, at a rate of 2 K/min, in order to directly compare DSC and BDS responses in the temperature domain. Finally, BDS measurements were

performed on selected samples during isothermal crystallization at temperatures in the region of crystallization, depending on the relaxation process under investigation. Continuous frequency isothermal scans taken every ~10 min provided an almost online view of changes in the dielectric response related to segmental dynamics during the evolution of the crystallization process [43–46].

BDS results were analyzed by fitting model functions [47] to the experimental data employing a proper software, in order to evaluate the time scale (temperature dependence of the frequency maxima of dielectric loss), the dielectric strength and the shape parameters of the recorded relaxations [42]. To that aim we employed the asymmetric Havriliak–Negami (HN) equation [47].

$$\varepsilon^*(f) = \varepsilon_\infty + \frac{\Delta\varepsilon}{\left(1 + (if/f_0)^{\alpha_{HN}}\right)^{\beta_{HN}}} \quad (4)$$

A sum of up to five HN terms of the type (4), one for each of the relaxations recorded (namely β, S, α, α_c, and α_{int}, details later in text), was critically fitted to the experimental data at each temperature and the fitting parameters were determined. The number of terms needed was different for different compositions and temperatures, depending on the number of relaxations present and the extent of their overlapping. In Eq. (4), $\Delta\varepsilon$ is the dielectric strength, f_0 is a characteristic frequency related to the frequency of maximum dielectric loss (ε''), ε_∞ describes the value of the real part of dielectric permittivity, ε', for $f \gg f_0$, and α_{HN} and β_{HN} are the shape parameters of the relaxation.

3. Results

3.1. Characteristics of materials under investigation

Results concerning the modification of silica A-380, before polymer adsorption have already been published [36] and they will be only briefly summarized here. A-380 consists of tightly packed spherical nanoparticles (~8 nm in diameter) forming aggregates of 100–500 nm [17]. The initiator of the zirconia synthesis ($Zi(acac)_3$) reacts with the free silanol (≡Si—OH) groups of silica (both in the inner and external surfaces) forming ≡Si—$Zi(acac)_3$ groups, upon which the zirconia nanoparticles were subsequently generated. According to FTIR, coverage of free silanols was not complete. It has been reported that zirconia suppresses, in general, the concentration of free hydroxyl groups in the modified A-380 particles [48].

According to XRD measurements [36], the 13–32 nm in diameter zirconia was found to be in the crystalline state, while its content was found equal to 5.9 wt% and 15.5 wt%, for 1 and 4 cycles of zirconia reaction, respectively (Table 1). The specific surface area, S_{BET}, of initial A-380, representative for the silica–polymer interaction area, was measured employing nitrogen adsorption–desorption isotherms [48] to 342 m^2/g. S_{BET} decreased to 262 m^2/g and, further, to 237 m^2/g after the 1st and 4th zirconia reaction cycle, respectively (Table 1) [36]. Mesopores (2 nm < diameter < 50 nm) and macropores (diameter ⩾ 50 nm) at the surfaces and voids of aggregates contribute mainly to the relatively high S_{BET} values. High S_{BET} for nanosilicas with mainly textural porosity (e.g. fumed silicas A-240, A-300, A-380 [28,39,48]) has been previously shown to describe well high degree of accessibility for both the gas molecules and the PDMS chains [12,13,17]. The decrease of S_{BET} after modification with zirconia was suggested to originate from the development of zirconia nanoparticles mainly onto the external silica surfaces, reducing this way their roughness.

3.2. Differential scanning calorimetry (DSC)

3.2.1. Protocol A

Fig. 1 presents comparative DSC thermograms in the glass transition region for silica/PDMS core–shell based nanocomposites and for neat PDMS, for measurements under *protocol A* (Fig. 1a and b) and for neat PDMS previously quenched (Fig. 1c). The overall cooling and subsequent heating DSC scans can be found in supplementary material SM.1. The crystallization of neat PDMS occurs during cooling at −76 °C and X_c ~0.65 wt (Table 2). Crystallization is almost absent during cooling for A380P40 and A380Z1P40, whereas X_c increases to ~0.13 for A380Z4P40 (Table 2). X_c increases significantly at the higher polymer loading (80 wt%, Table 2).

During the heating in measurements of *Protocol A*, in Fig. 1, all samples demonstrated single glass transition steps in the region between −140 °C and −115 °C, with T_g values between −135 °C (A380Z4P40) and −127 °C (neat PDMS) (Table 2). The

Table 1
Textural and porosity characteristics of unmodified A-380 and modified A-380/ZrO_2 oxides as taken from previous study [36]. Z1 and Z4 correspond to 1 and 4 reaction cycles of zirconia grafting, respectively. Zirconia content according to XRD, C_{ZrO2}, specific surface area as recorded by Nitrogen adsorption–desorption isotherms, S_{BET}, average volume of pores, V_p, of mesopores (details in text), V_{meso}, and of macropores, V_{macro}.

Oxide	C_{ZrO2} (wt.%)	S_{BET} (m^2/g)	V_p (cm^3/g)	V_{meso} (cm^3/g)	V_{macro} (cm^3/g)
A380 unmodified	0	342	1.160	0.311	0.849
A380Z1	5.9	262	1.996	0.142	1.854
A380Z4	15.5	237	1.186	0.390	0.796

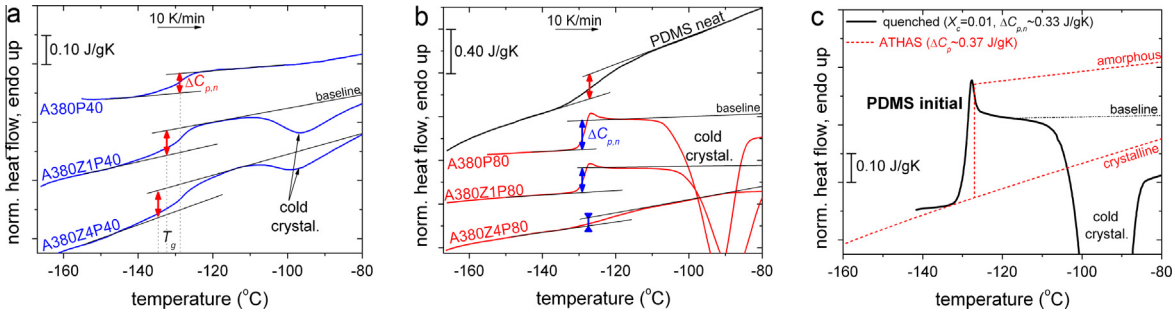

Fig. 1. Comparative DSC thermograms in the glass transition region of samples of (a) 40 wt% and (b) 80 wt% PDMS adsorbed onto unmodified and modified A-380, and for comparison for neat PDMS in (b), for measurements of *Protocol A*. The curves of DSC heat flow are normalized to amorphous polymer mass and to heating rate and, thus, are presented in specific heat capacity, C_p, units. The added lines represent the baselines of the thermograms before and after glass transition. The distance between these two baselines at the glass transition temperature, T_g, is taken as the absolute value of change in heat capacity, $\Delta C_{p,n}$ (Table 2) for each sample. (c) shows the DSC thermograms in the glass transition region of initial amorphous PDMS during heating at 10 K/min of a sample previously cooled at ~90 K/min (quenched, solid line). Results for C_p of PDMS against temperature taken from ATHAS databank [49] are comparatively shown in (c) (dashed lines).

Table 2
Quantities of interest from DSC measurements of *Protocols A and AC*: crystallization temperature, T_c, glass transition temperature, T_g, normalized heat capacity step of glass transition, $\Delta C_{p,n}$, temperature maxima of melting, $T_{m1,2}$, normalized melting enthalpy $\Delta H_{m,n}$, degree of crystallinity, X_c, rigid and mobile amorphous polymer fractions, *RAF* and *MAF*, respectively. Note: X_c, *RAF* and *MAF* refer to whole polymer mass (i.e. X_c + *RAF* + *MAF* = 1).

Protocol	Sample	T_c (°C) (±0.5)	T_g (°C) (±0.5)	$\Delta C_{p,n}$ (J/g K) (±0.02)	T_{m1} (°C) (±0.2)	T_{m2} (°C) (±0.2)	$\Delta H_{m,n}$ (J/g) (±1)	X_c (wt) (±5%)	*RAF* (wt) (±10%)	*MAF* (wt) (±10%)
Protocol A	A380P40	–	−129	0.07	−48	–	0	0.00	0.79	0.21
	A380Z1P40	−103	−133	0.09	−50	–	3	0.01	0.72	0.27
	A380Z4P40	−95	−135	0.09	−50	–	8	0.13	0.63	0.24
	A380P80	−98	−129	0.28	−48	−39	22	0.08	0.14	0.78
	A380Z1P80	−97	−129	0.22	−49	−40	19	0.05	0.32	0.63
	A380Z4P80	−90	−128	0.07	−49	−40	19	0.45	0.43	0.12
	PDMS	−76	−127	0.22	−47	−40	24	0.65	0.12	0.23
Protocol AC	A380P40	–	−129	0.09	–	–	0	0.00	0.73	0.27
	A380Z1P40	–	−129	0.03	−50	–	5	0.12	0.80	0.08
	A380Z4P40	–	−127	0.04	−51	–	9	0.23	0.67	0.10
	A380P80	–	−122	0.15	−47	−39	23	0.61	0.21	0.18
	A380Z1P80	–	−121	0.02	−50	−40	19	0.52	0.45	0.03
	A380Z4P80	–	−122	0.02	−51	−40	19	0.51	0.46	0.03
	PDMS	–	−126	0.15	−46	−40	25	0.67	0.18	0.15

value for neat PDMS is in agreement with previous studies of PDMS [9,12,41,44]. Interestingly, T_g of the core–shell systems is by 2 K lower than that of neat PDMS and it is further reduced on addition of nanozirconia by 1–8 K. $\Delta C_{p,n}$ for nanocomposites of 40 wt% PDMS is smaller than for neat PDMS. A slight increase is observed in nanocomposites with zirconia modification. On the other hand, for A380P80 $\Delta C_{p,n}$ value is larger as compared to neat PDMS.

As temperature increases above T_g during heating, an exothermic event was observed in the case of A380Z1P40, A380Z4P40 and all nanocomposites of 80 wt% PDMS loading (Fig. 1), representing cold crystallization, a phenomenon which follows uncompleted crystallization during cooling [50,51].

At higher temperatures, complex endothermic melting peaks are observed between −48 and −39 °C (T_{m1}, T_{m2} in Table 2, supplementary material SM.1). In consistency with cooling thermograms, melting is absent for A380P40 and quite weak for A380Z1P40 and A380Z4P40. Strong double melting peaks are observed for all nanocomposites of 80 wt% PDMS. As discussed in previous work [18,41] events of recrystallization and melting contribute in the temperature region of melting. For that reason, in measurements of *Protocol A* the degree of crystallinity was not calculated from the melting enthalpy. Nevertheless, the melting enthalpy normalized to the same polymer fraction, $\Delta H_{m,n}$, is lower in the nanocomposites than in neat PDMS (Table 2).

3.2.2. Protocol AC

Fig. 2 shows DSC thermograms in the glass transition region during heating after a 20 min annealing of crystallization (*Protocol AC*, details in Section 2.2). We should note that the annealing temperature was different for different samples, aiming at maximum degree of crystallinity. Obviously, this affects the evolution of crystallization and the structure of polymer

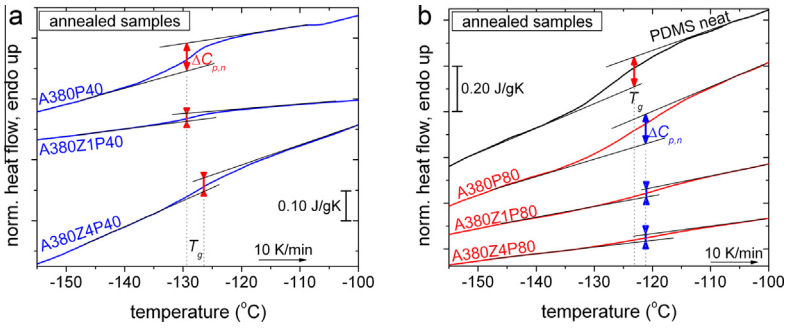

Fig. 2. Comparative DSC thermograms in the glass transition region of (a) 40 wt% PDMS and (b) 80 wt% PDMS adsorbed in unmodified and modified A-380, and for comparison of neat PDMS. Results are shown for measurements of *Protocol AC* (i.e. annealed samples) during heating. The curves of DSC heat flow are normalized to amorphous polymer mass and to heating rate and, thus, are presented in specific heat capacity, C_p, units. The added lines represent the baselines of the thermograms before and after glass transition. The distance between these two baselines at the glass transition temperature, T_g, is taken as the absolute value of change in heat capacity, $\Delta C_{p,n}$ (Table 2) for each sample.

crystals [50,51]. In the case of annealed samples X_c was estimated employing the normalized melting enthalpy, $\Delta H_{m,n}$, in Eq. (2). Results were analyzed and evaluated and the respective values of interest are shown in Table 2.

Crystallization was again absent for A380P40, while T_g remained the same as in *Protocol A*. Interestingly, $\Delta C_{p,n}$ was slightly increased from 0.07 to 0.09 J/gK (Table 2). With the exception of A380P40, crystallization annealing resulted in increased degree of crystallinity for all samples, significantly higher for samples of 80 wt% PDMS loading. T_g increased slightly on annealing for 40 wt% PDMS samples, still remaining lower than that of neat PDMS (Fig. 2a, Table 2). On the other hand, T_g for nanocomposites of 80 wt% PDMS increased strongly to values higher than in neat PDMS (Fig. 2b, Table 2).

Summarizing the findings from DSC, the interaction between A-380 and the polymer in the core–shell systems suppresses highly the crystallization ability of PDMS, which is in general extremely weak for the 40 wt% PDMS content, while glass transition is enhanced (T_g decreases, $\Delta C_{p,n}$ increases). Annealing procedure increases either $\Delta C_{p,n}$ or X_c (Table 2). In the case of high polymer content, zirconia modification suppresses glass transition (T_g increases, $\Delta C_{p,n}$ decreases) and enhances simultaneously crystallization. Similar effects are caused by thermal annealing. Effects imposed here by annealing and surface modification on the thermal transitions of the polymer, resemble those imposed on polymer melts adsorbed on solid surfaces [32,35] or confined to spatial dimension of the nanometric scale [33,34] and discussed in terms of recorded changes in adopted conformations by polymer chains at interfaces [3,29,33,35]. Such a relation [17,27] will be employed also in this work, later in the discussion section.

3.2.3. Evaluation of polymer fractions according to calorimetric response

In many previous studies on various polymer nanocomposites, including polymer–silica nanocomposites, DSC results have often showed no significant variation of T_g with filler fraction along with the reduction ΔC_p [8]. The results have been interpreted in terms of a Rigid Amorphous Fraction, *RAF* [52], being immobilized on the surface of the well-dispersed nano-inclusions thus making no contribution to the glass transition [53] and references therein. Furthermore, the deviation of ΔC_p of nanocomposites from that of the neat polymer proved a good measure of the degree of polymer–filler interaction [52,53]. On the other hand, the fraction of polymer which contributes to glass transition makes the Mobile Amorphous Fraction, *MAF* [52]. Thus, a '2-phase model' (*MAF* + *RAF*) has been previously employed for nanocomposites based on amorphous polymers [53], while an additional Crystalline Fraction, *CF* ($\sim X_c$), coexists in the '3-phase model' (i.e. *CF* + *MAF* + *RAF*) for semi-crystalline neat polymers [52]. For nanocomposites based on semicrystalline polymers the situation is more complex, as for $X_c = 0$, *RAF* represents the immobilized polymer at the particles–polymer interfaces (i.e. $RAF = RAF_{int}$), whereas for $X_c \neq 0$, *RAF* should also include the rigid amorphous polymer part immobilized in close proximity to polymer crystals [52,54] (i.e. $RAF = RAF_{int} + RAF_{cryst}$). It has been suggested that RAF_{cryst} does not relax during glass transition [52,55] or that its relaxation may occur at temperatures close to melting, T_m, i.e. significantly higher than T_g of the bulk [54].

In the present study we categorize and evaluate the different polymer phases with respect to the type of their contribution to glass transition. Thus, we first estimated the amount of polymer which contributes to amorphous mobility, *MAF*, according to Eq. (5),

$$MAF = \frac{\Delta C_{p,n}}{\Delta C^{PDMS}_{p,amorphous}}(1 - X_c) = \frac{\Delta C_{p,n}}{0.33(\mathrm{J/gK})}(1 - X_c) \quad (5)$$

where $\Delta C^{PDMS}_{p,amorphous}$ is the $\Delta C_{p,n}$ of fully amorphous unaffected PDMS, found equal to 0.33 J/gK via fast cooling measurements (quenching, Fig. 1c). According to the widely used ATHAS Database [49], ΔC_p of amorphous PDMS (in general over the various types) is equal to 0.37 J/gK (Fig. 1c), quite similar to our result. Bearing in mind that molecular dynamics of a polymer is related to its physical properties (e.g. chain-end groups, crosslinking density etc.) [50], we will use our experimental value (0.33 J/gK) for further calculations related to glass transition.

According to our calculations (Table 2), the sum of mobile amorphous and crystallized polymer fractions ($MAF + X_c$) is lower than 1 in the nanocomposites, suggesting that, in the frame of the '3-phase model', one part of the response is missing from the calculated fractions. This deviation is thought to represent *RAF*, which can be easily calculated by Eq. (6).

$$RAF = 1 - X_c - MAF \tag{6}$$

The calculated fractions of various polymer phases are included in Table 2, for measurements under both protocols. We should remind that all fractions refer to whole polymer mass according to the above equations employed for DSC. According to Schick and coworkers [53,55] in nanocomposites based on semicrystalline polymers, the RAF_{cryst} to X_c and RAF_{cryst} to RAF_{int} ratios may not be constant in DSC. Additionally, we have demonstrated that the interfacial polymer fraction can be temperature dependent according to BDS [17]. Therefore, we will not attempt to calculate separately these fractions and we will consider results by Eqs. (5) and (6) as simplified approximations for *MAF* and *RAF* at temperatures close to T_g.

The sum of X_c and *MAF* is higher for 80 wt% PDMS, while, as expected, *RAF* is higher for samples of 40 wt% PDMS. In addition, from a first glance in Table 2, the above fractions change systematically with zirconia modification (X_c + *MAF* increases and *RAF* decreases), while, changes of *RAF* for low polymer adsorption (no significant interference of crystallinity) seem to follow the respective changes of S_{BET} (Table 1). These effects will be discussed later in comparison with respective BDS results.

3.3. Broadband dielectric spectroscopy (BDS)

3.3.1. Raw data and analysis

BDS results will be comparatively presented here in the form of frequency dependence of the imaginary part of dielectric permittivity, ε'' (Fig. 3, isothermal plots). The main focus is on segmental dynamics, i.e. on the dielectric relaxations corresponding to the DSC response in the region of glass transition in Figs. 1 and 2 (namely α, α_c and α_{int}). The dielectric response was found significantly higher for the samples containing 40 wt% PDMS as compared to 80 wt% PDMS (Fig. 3). This difference is confirmed also by the results for the real part of dielectric permittivity, ε', and AC conductivity, σ_{AC}, (not shown).

After analysis of the complex BDS spectra (details in Section 2.3), the plots of Figs. 4 and 5 were constructed, by plotting f_{max} and $\Delta\varepsilon$ of the three segmental and the two local (β and *S*) relaxations against reciprocal temperature. Included in the Arrhenius plots of Figs. 4a and 5a are results by DSC and TSDC (raw data not presented here), namely glass transition temperatures and peak temperatures, respectively, at the equivalent frequencies of the techniques, 20 mHz and 1.6 mHz, respectively [8]. TSDC (Thermally Stimulated Depolarization Currents) [56] is a special dielectric technique in the temperature domain [8,17,40]. Selected BDS results will be shown here also in the form of temperature dependence of ε'' (Fig. 6, isochronal plots).

3.3.2. Interfacial relaxation

α_{int} relaxation in Fig. 3a and b, located in the broad range from 10 to $2 \cdot 10^2$ Hz at −80 °C, represents the dynamics of polymer chains in the interfacial layer, with strongly reduced mobility due to interactions with the surface hydroxyls of A-380 [9,17]. Over the last years we studied in detail interfacial dynamics in polymer nanocomposites based on poly(dimethylsiloxane) (PDMS) and natural rubber (NR) as matrices and silica or titania as fillers, prepared by sol–gel techniques in the presence of the cross-linked polymer matrix [8,9,40]. More recently, this work has been extended to nanocomposites, where PDMS has been physically adsorbed from a solution onto nano-oxides in powder form [17,27], such as in the present work. A methodology based on DSC and dielectric techniques to study segmental dynamics in nanocomposites revealed the presence of a slower segmental relaxation (i.e. α_{int} here) in the interfacial layer, next to the bulk segmental relaxation. This slower dynamics has been attributed to the polymer–filler interaction, namely the formation of hydrogen bonding [57,58] between the oxygens on the polymer backbone of PDMS and the hydroxyls on the nanoparticles surface [9,17]. Except for the presence of α_{int} only in the nanocomposites, we have recorded that its magnitude increases in general with filler content [8,18,40], and with specific surface area of initial particles [17,27], while its time scale behavior resembles that of segmental (cooperative) polymer dynamics.

The temperature dependence of segmental dynamics is typically described by Vogel–Tammann–Fulcher–Hesse (VTFH) equation [59],

$$f = f_0 \exp\left(-\frac{DT_0}{T - T_0}\right) \tag{7}$$

where f_0 is a frequency constant, *D* is the strength parameter, and T_0 is the Vogel temperature. After fitting Eq. (7) to our experimental data and fixing the f_0 parameter to the phonon value 10^{13} Hz [42,60], we obtained values for T_0 and *D*. *D* is related to the steepness or fragility index *m* according to the following equation [61]

$$m = 16 + 590/D \tag{8}$$

The fragility (cooperativity) index values for all segmental relaxations (α_{int}, α_c and α) were calculated and are listed in Table 3.

From a first glance at the Arrhenius plots (Figs. 4a and 5a), the time scale of α_{int} relaxations seems to tend to more linear-like (Arrhenius, constant activation energy) behavior as compared to α and α_c, especially as zirconia grafting increases.

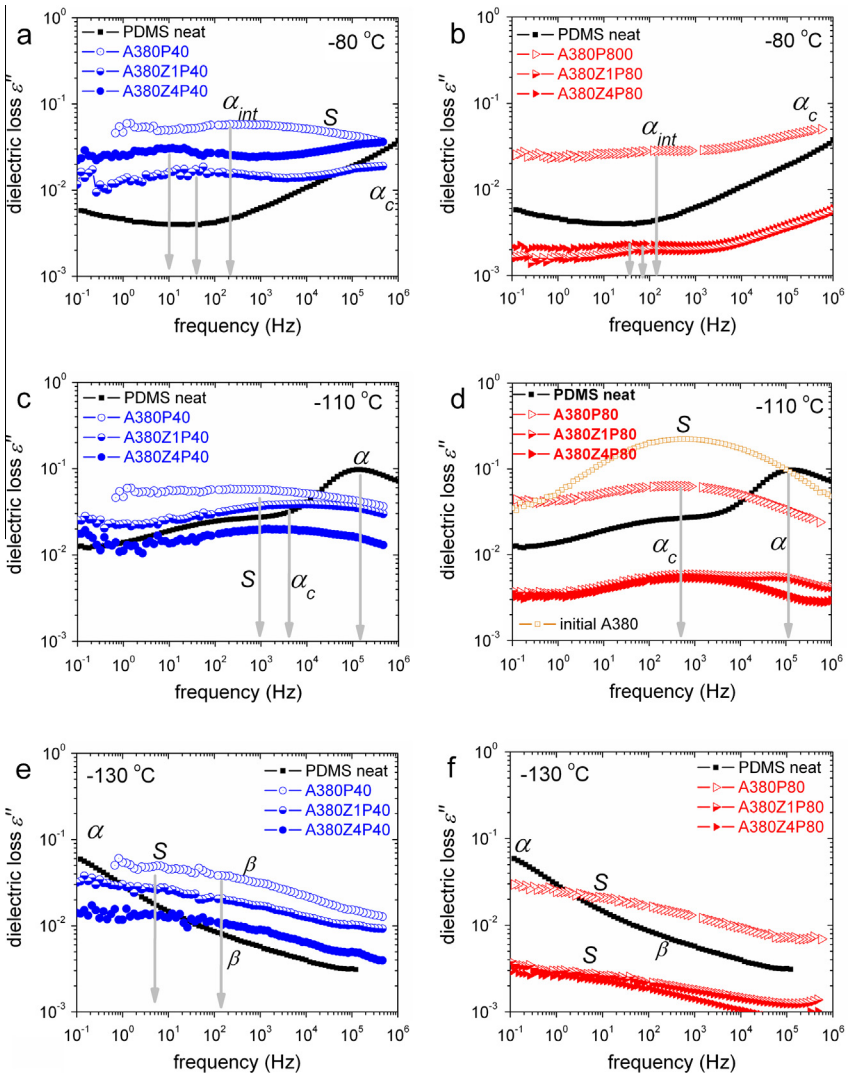

Fig. 3. Isothermal BDS plots of the imaginary part of dielectric permittivity, ε'', vs frequency for PDMS and the composites with (a, c, e) 40 and (b, d, f) 80 wt% adsorbed PDMS, at −80, −110 and −130 °C. Results are shown for measurements of thermal *Protocol A*. Indicated are the dielectric relaxations related to segmental and local dynamics. Results for initial A-380 (*S* relaxation) at −110 °C have been included in (d).

Additionally, α_{int} becomes slower, while its strength (Figs. 4b and 5b) and cooperativity (*m* in Table 3) are reduced with zirconia modification (addition of ~6 and ~16 wt% zirconia, Table 1). The strength of α_{int} is smaller for composites with 80 wt% PDMS (Fig. 5b), as compared to 40 wt% PDMS (Fig. 4b). The respective changes with zirconia modification are more pronounced for the samples of the low polymer loading.

3.3.3. Bulk-like relaxations

α relaxation in Fig. 3c and d at around 10^5 Hz at −110 °C is associated with the glass transition of the amorphous unaffected (bulk) polymer fraction [9,17,40], observed only in neat PDMS and A380Z1P80. This relaxation corresponds to the lower temperature sharp-shaped glass transition step in DSC (Fig. 1b and c). Next to α, at around (10^3 Hz, −110 °C), α_c relaxation originates from polymer chains restricted either between condensed crystal regions [9,44] (i.e. case of neat and 80 wt% PDMS, Fig. 3d) or in the voids between nanoparticles in their aggregates (i.e. case of core–shell nanocomposites at low polymer loading, Fig. 3c) [17,62]. The dynamics of each of these relaxations is almost identical in the nanocomposites and in neat PDMS in Figs. 4a and 5a.

Additional support about the origin of α_c and α relaxations is provided by isochronal measurements. Data recorded isothermally were comparatively replotted in Fig. 6 as isochronal $\varepsilon''(T)$ plots to facilitate direct comparison with the DSC thermograms of Figs. 1 and 2. The frequency of 121 Hz was selected as representative for this comparison. Despite the fact that these diagrams are not real isochronal measurements but replottings of isothermals, the results are not far from reality,

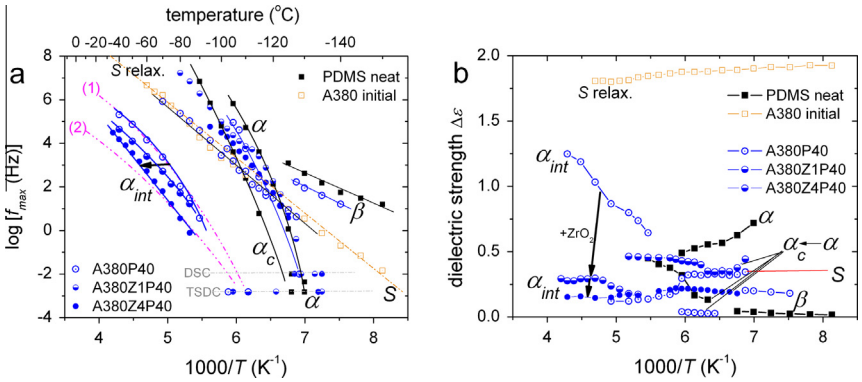

Fig. 4. (a) Arrhenius plots and (b) dielectric strength vs reciprocal temperature of the local (β, S) and segmental bulk (α), constrained in voids or/and between polymer crystals (α_c) and interfacial (α_{int}) dynamics for initial A-380, neat PDMS, A380P40 [17], A380Z1P40 and A380Z4P40 recorded in isothermal BDS measurements under thermal *Protocol A*. Respective DSC and TSDC data have been added in (a). The lines in (a) are fittings of the Arrhenius and the VTFH equations (details in text). The arrows mark changes in α_{int} relaxation imposed by zirconia modification of grafting on the initial A-380 particles. Lines (1) and (2) in (a) correspond to the interfacial relaxation in conventional PDMS/silica and PDMS/titania nanocomposites, respectively [9].

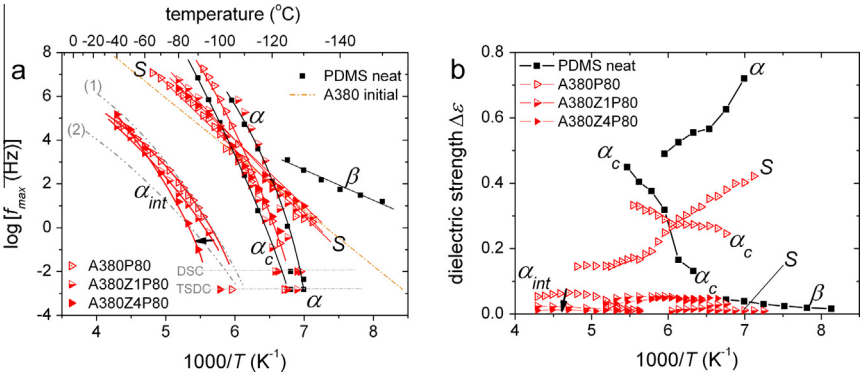

Fig. 5. (a) Arrhenius plots and (b) dielectric strength vs reciprocal temperature, of the local (β, S) and segmental bulk (α), constrained in voids or/and between polymer crystals (α_c) and interfacial (α_{int}) dynamics for initial A-380, neat PDMS, A380P80 [17], A380Z1P80 and A380Z4P80 recorded in isothermal BDS measurements under thermal *Protocol A*. Respective DSC and TSDC data have been added in (a). The lines in (a) are fittings of the Arrhenius and the VTFH equations (details in text). The arrows mark the changes in α_{int} relaxation imposed by zirconia modification on the initial A-380 particles. Lines (1) and (2) in (a) correspond to the interfacial relaxation in conventional PDMS/silica and PDMS/titania nanocomposites, respectively [9].

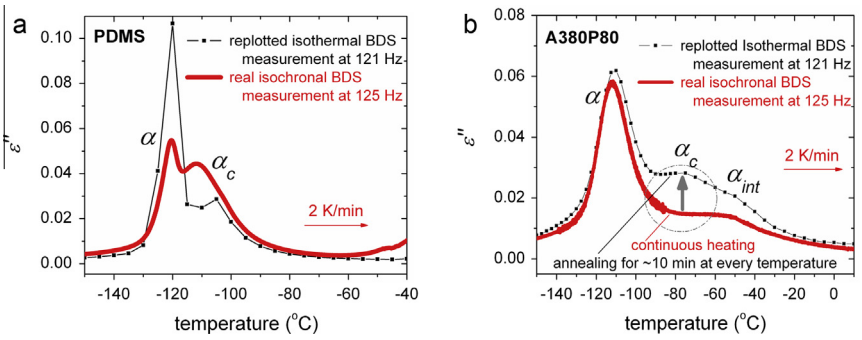

Fig. 6. Comparative isochronal plots of the imaginary part of dielectric permittivity, ε'', replotted from BDS isothermal measurements at 121 Hz (black pointed curves) and directly measured at 125 Hz (red solid curves), for (a) neat PDMS and (b) A380P80. Indicated are the recorded relaxations. (For interpretation of the references to color in this figure legend, the reader is referred to the web version of this article.)

as confirmed by comparison with real isochronal DRS measurements at 125 Hz for pure PDMS (Fig. 6a) and A380P80 (Fig. 6b). The results are consistent with those of DSC regarding T_g, the shifts of α and α_c relaxations to higher temperatures in Fig. 6, as compared to Figs. 1 and 2, arising from the higher frequency of presentation [8].

Table 3
Shape parameters of the fitted HN equation (Section 2.3, Eq. (4)) a_{HN} and β_{HN} (average over temperature), fragility index, m, for the recorded dielectric segmental relaxations, and interfacial polymer fraction at −95 °C, RAF_{int} (Eq. (10)). (∗) corresponds to relaxations that do not obey VTFH equation.

Process	α (*Protocol A*)			α_c (*Protocol A*)			α_{int} (*Protocol A*)				α_{int} (*Protocol AC*)			
Parameter / Sample	a_{HN}	β_{HN}	m	a_{HN}	β_{HN}	m	a_{HN}	β_{HN}	m	RAF_{int} (vol)	a_{HN}	β_{HN}	m	RAF_{int} (vol)
A380P40	–	–	–	–	–	–	0.26	1	43	0.86	0.24	1	∗	0.55
A380Z1P40	–	–	105	0.23	1	92	0.30	1	34	0.34	0.28	1	31	0.22
A380Z4P40	–	–	–	0.21	1	∗	0.26	1	32	0.23	0.25	1	31	0.16
A380P80	–	–	–	0.44	1	102	0.45	1	52	0.05	0.30	1	38	0.02
A380Z1P80	0.41	0.9	122	0.24	1	87	0.30	1	36	0.27	0.30	1	35	0.14
A380Z4P80	–	–	–	0.33	1	67	0.37	1	32	0.13	0.35	1	33	0.10
PDMS	0.43	0.9	106	0.30	1	96	–	–	–	0.00	–	–	–	0.00

A further comment refers to the different recordings of α_c relaxation Fig. 6b. In the case of A380P80, we recall from the DSC data (Table 2) that the presence of silica in A380P80 suppresses strongly the degree of crystallinity, X_c (0.08), and T_c (−98 °C) in Table 2. Thus, we expect that α_c relaxation should be absent in a continuous heating measurement at 2 K/min. This is true in fact in the real isochronal measurements of Fig. 6b. In the case of the isochronal replottings, the ∼10 min isothermal annealing of the sample at each temperature of measurement, including the T_c region, necessary for stabilizing the temperature and for scanning the frequency range of measurements, led to the arising of α_c relaxation. Thus, the sample is more amorphous in the real isochronal measurements in Fig. 6 as compared to the isochronal replottings of the BDS measurements. The situation is different for neat PDMS in Fig. 6a, due to the higher crystallization temperature of the neat polymer (−76 °C in Table 2) and the already high degree of crystallization (∼0.65 in Table 2).

Effects of nanozirconia and filler content on the bulk-like relaxations (mainly on their strength in Figs. 4b and 5b, and cooperativity, m, in Table 3) are indirect and mainly expressed via the changes induced on the degree of crystallinity (Table 2), in agreement to previous studies of PDMS [17,18,44].

3.3.4. Local relaxation of —OH groups on silica surface

S relaxation [63] located at around (10^3 Hz, −110 °C) in Fig. 3d, is related with motions of the silanol surface groups of silica (Si—OH) with attached water molecules [63,64]. We observe in Fig. 3d that the *S* relaxation dominates the response for initial silica A-380 (with ambient hydration of about 10 wt%). After careful analysis of the results, *S* shows exactly the same time scale with the *S* relaxation measured in A380P40 and all nanocomposites of 80 wt% PDMS loading. As expected, $\Delta\varepsilon$ of *S* is lower in the nanocomposites than in neat A-380 (Figs. 4a and 5a). In our previous studies on similar core–shell systems, it has been demonstrated that *S* relaxation becomes weaker as the degree of polymer adsorption (surface coverage of the particles) increases [12,13,17]. In work in progress on nanocomposites based on PDMS (the same and similar with those in the present study) we obtain similar results imposed by water content, in particular, an increase in the dielectric strength of *S* relaxation with increasing hydration level.

3.3.5. Secondary (local) polymer relaxation

A faster but relatively weak relaxation is located at around 100 Hz at −130 °C in Fig. 3e. The relaxation named here 'β', has not been reported in previous work in PDMS, focusing however on segmental dynamics [8,44,65]. Analysis of the results shows that β ($\alpha_{HN} \sim 0.23$, $\beta_{HN} = 1.0$): (i) obeys Arrhenius equation [66] (i.e. linear trace in Fig. 4a, activation energy ∼0.26 eV), (ii) is weaker by one order of ε'' magnitude as compared to segmental relaxations in Fig. 4b, and (iii) slightly increases in dielectric strength with temperature (Fig. 4b). According to Ngai [67] these characteristics suggest that β is a local (secondary) relaxation of the polymer. In consistency with that, β relaxation shows quite similar behavior in the nanocomposites (whenever recorded, depending on the availability and the quality of low temperature measurement) as in the case of initial PDMS. The limited information available at present (only a few points in Figs. 4 and 5) precludes at this stage a more detailed study of the relaxation in terms of Johari–Goldstein type [68] or local relaxation [67]. More work is need to further clarify the molecular origin of the relaxation, for example by studying PDMS of (i) different structure (linear, crosslinked) and (ii) various molecular weights in order to conclude as to whether the relaxation recorded here is related to the concentration of chain ends of PDMS or not. In addition, employing a comparison with polymers similar to PDMS (—CH_3 side groups) but of modified chemical structure, such as poly(methylphenylsiloxane) (PMPS, —C_6H_5 side groups), could be also illuminating regarding local relaxation matters.

3.3.6. Evaluation of polymer phases according to dielectric response

The results reported in the previous sections provide clear evidence about the origin of the various segmental relaxations. Thus, we may calculate the various fractions of polymer by evaluating the respective dielectric responses (i.e. $\Delta\varepsilon$). To that aim we employ a model analogue to the one used previously for DSC (i.e. Eqs. (5) and (6)) and we calculate the mobile bulk, *MAF*, and the interfacial, RAF_{int}, polymer fractions according to the following equations

$$MAF = \frac{\Delta\varepsilon_{a+ac}}{\Delta\varepsilon_a + \Delta\varepsilon_{ac} + \Delta\varepsilon_{a\,int}}(1 - X_c) \quad (9)$$

$$RAF_{int} = \frac{\Delta\varepsilon_{a\,int}}{\Delta\varepsilon_a + \Delta\varepsilon_{ac} + \Delta\varepsilon_{a\,int}}(1 - X_c) \quad (10)$$

where $\Delta\varepsilon$ is the dielectric strength [42] of each relaxation and X_c is the degree of crystallinity for each sample (obtained from DSC, Table 2). Bearing in mind that the dielectric strength changes with temperature, we employed BDS results at the same temperature −95 °C for *MAF* and RAF_{int}. Results of RAF_{int} are shown in Table 3. They show that RAF_{int} is reduced with surface modification from 0.86 to 0.23 wt for samples of 40 wt% PDMS. RAF_{int} is weaker, as expected, for higher polymer adsorption (80 wt%) and changes with surface modification are not systematic. The results will be discussed later comparatively with those obtained by DSC (Table 2).

From the methodological point of view, Eqs. (9) and (10) involve the total dielectric response of the segmental relaxations for each sample. Thus, we may assume that any systematic errors in the calculations and the comparison between different samples, arising from possible differences in polarizability of PDMS chains in the different fractions [22], are reduced by this calculation method. As mentioned above, the lower dielectric response of the 80 wt% PDMS nanocomposites as compared to the 40 wt% nanocomposites (Fig. 3) can explain the lower values of RAF_{int} for the samples of 80 wt% PDMS (Table 3). On the other hand, we recall that the respective equations employed for DSC compare the response of nanocomposites with that of initial polymer, the two methods being different in principle. The suitability of Eqs. (9) and (10) for calculating the different polymer fractions has been confirmed in NCs based on silica and various polymers [10,11,16,27].

3.3.7. Effects of thermal (crystallization) treatment

We turn now attention to the effects of crystallization annealing on α_{int} relaxation. To that aim, we compare in Fig. 7 results of measurements under standard treatment (*Protocol A*) and annealing of crystallization before the BDS measurements (*Protocol AC*) for samples of low polymer loading. Similar results were obtained also for samples at high polymer loading (not shown here). We recall that previously in Fig. 4 we showed effects on molecular dynamics imposed by zirconia modification on the nanocomposites of low polymer loading. Thus, now in Fig. 7 effects induced by annealing and the combination of annealing and surface modification of silica are comparatively shown. In addition, we show and evaluate in Fig. 8 online measurements during isothermal annealing.

It becomes clear that annealing of crystallization leads in general to slower α_{int} relaxation (Fig. 7a), with lower dielectric strength (Fig. 7b), suppressed fragility (m) and RAF_{int} (Table 3) for both polymer loadings. The effects imposed by annealing on α_{int} become gradually weaker with increasing of surface modification. Paralell to changes imposed on α_{int} by annealing, α_c relaxation tends also to become slower (Fig. 7a), whereas its strength increases (Fig. 7b).

In Fig. 8 we demonstrate an online time-monitoring of the effects imposed by isothermal annealing on segmental dynamics in neat PDMS at −114 °C (Fig. 8a) and in A380P80 at −85 °C (Fig. 8b). The response of the initially highly crystallized neat PDMS ($X_c \sim 0.65$ wt at the beginning and ~0.75 wt at the end) was expressed via both α and α_c relaxations in Fig. 8a, while during isothermal annealing α_c becomes stronger and α weaker. The recordings are similar to those in previous studies of PDMS [9,44]. Analysis showed that the total dielectric strength ($\Delta\varepsilon_{\alpha+\alpha c}$) decreased with annealing time (inset to Fig. 8a). Moreover, $\Delta\varepsilon_{\alpha+\alpha c}$ was decreased by a factor of about 2 at the end of annealing, while the degree of crystallinity increased by only ~15 wt%. This would suggest that the growth and interference of a rigid amorphous fraction due to the polymer

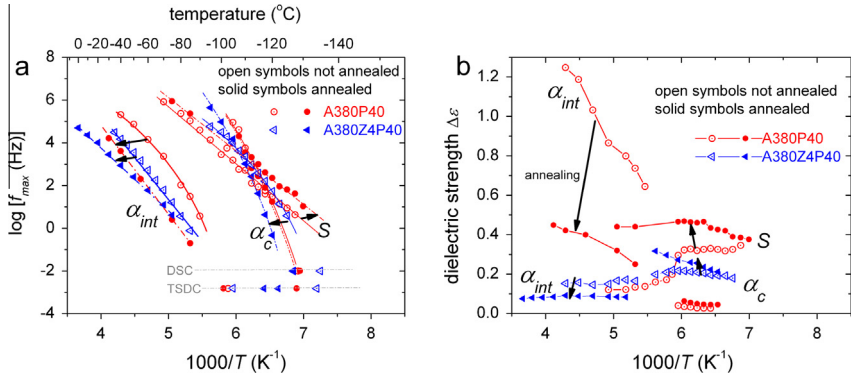

Fig. 7. Comparative (a) Arrhenius plots and (b) dielectric strength vs reciprocal temperature of the local (S), segmental bulk-like (α_c), and interfacial polymer dynamics (α_{int}) for A380P40 (cycles) [17] and A380Z4P40 (triangles) composites, recorded in isothermal BDS measurements under thermal *Protocols A* (open symbols) and *AC* (solid symbols). Respective DSC and TSDC data have been added in (a). The lines in (a) are fittings of the Arrhenius and the VTFH equations. The arrows mark changes induced by annealing.

crystallites, RAF_{cryst}, [52,55] is significant also in the nanocomposites, especially in the case of high PDMS loading. In the case of A380P80, X_c was increased from 0.08 to 0.61 during the annealing at −85 °C (Table 2) and at the same time α_c remained almost unchanged (weakly suppressed) in Fig. 8b. Interestingly, α_{int} relaxation became weaker during annealing (inset to Fig. 8b) and shifted to lower frequencies, in agreement also to the results in Fig. 7. Taken together the results for neat PDMS and A380P80 in Fig. 8 provide additional evidence that α_{int} does not represent the relaxation of RAF_{cryst}, but is directly related to RAF_{int}.

4. Discussion

4.1. Polymer crystallization

Independently of surface modification and thermal treatment, the presence of A-380 results in reduction of crystallization temperature, T_c, and degree of crystallinity, X_c, as compared to neat PDMS (Table 2). These results suggest that the particles/aggregates do not act as crystallization nuclei [50]. Crystallization during cooling is absent in the cases of composites with 40 wt% PDMS, due to the strong polymer–filler interaction (hydrogen bonding) which gives birth to significant amount of interfacial polymer fraction [8] close to the nanoparticles according to both DSC and BDS. Interfacial polymer affects negatively the ability of bulk polymer to form crystals, due to suppression of chain mobility/diffusion [9] and/or of the available (free) volume in the nanocomposites [21,23]. It has been pointed out that the crystallization process can be the driving force for rearrangement of nanoparticles distribution in a polymer matrix [69]. This is compatible with our findings for the 80 wt% PDMS samples, as the polymer matrix consists of linear polymer of low viscosity (~1000 cPS) and high crystallization ability ($X_c \sim 0.5$–0.8 wt [9,41]) and the distribution of the quite large A-380 aggregates (~300 nm [17]) could change during the growing of the even larger PDMS spherulites (~10^2 μm in size [70]).

4.2. Glass transition

Glass transition of the bulk was recorded extremely weak for samples of low polymer adsorption (40 wt% PDMS). T_g was lower in all cases of nanocomposites, dominated by: (a) spatial confinement effects [65,71] in case of lower PDMS loading and (b) suppressed X_c in case of higher PDMS loading. For samples of high PDMS adsorption (80 wt%), T_g increases due to higher X_c in Table 2, since physical and spatial constraints imposed by the spherulites [70] hinder the diffusion of polymer chains [44,50,62]. Annealing of crystallization of the composite samples results in further suppression of bulk dynamics, increasing X_c and T_g (Table 2).

Independently of the changes in T_g, the presence of a rigid amorphous polymer fraction (immobile according to DSC [53]), most probably located at the interfaces with A-380, is manifested by the suppression of $\Delta C_{p,n}$ in the nanocomposites (Table 2). According to commonly employed equations (Eqs. (5) and (6)), this fraction (*RAF*) was estimated around 0.8 wt of the whole polymer mass in A380P40 (Table 2). *RAF* decreases with surface modification down to ~0.6 wt (Fig. 9a). As expected, this decrease of interfacial polymer results in an increase of bulk-like polymer (i.e. *CF* + *MAF*, Fig. 9a). *RAF* calculations in samples of $X_c \neq 0$ on the basis of DSC include also the rigid amorphous polymer due to crystallites (RAF_{cryst}) [52,54], with the effect that the results of thermal annealing on *RAF* are controversial in Fig. 9a. Thermal annealing imposes an interplay between $CF + MAF + RAF_{cryst}$, on the one hand, and RAF_{int}, on the other hand. The situation becomes more clear in BDS results which follow (Fig. 9b, next section).

4.3. Bulk-like dynamics (α and α_c relaxations)

Exploiting the high resolving power of BDS technique, the dielectrically active polymer phases (i.e. bulk-like and interfacial) could be evaluated in the nanocomposites (Fig. 9b).

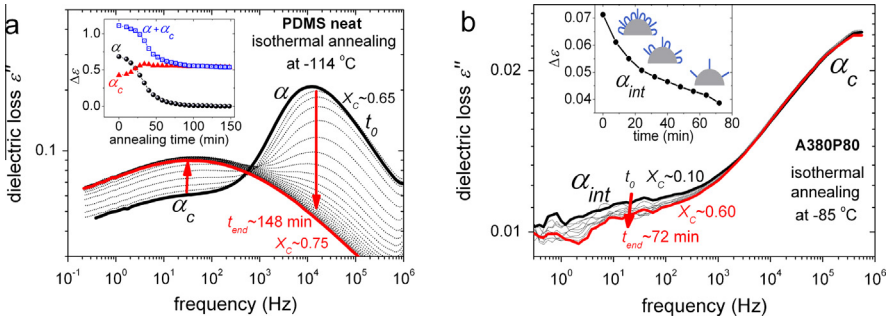

Fig. 8. Time evolution of the dielectric relaxation mechanisms associated to segmental dynamics during the isothermal crystallization annealing, for (a) neat PDMS at −114 °C and (b) A380P80 at −85 °C. Indicated in (a and b) are the estimated degree of crystallinity values, X_c, according to DSC, at the beginning, t_0, and at the end, t_{end}, of the annealing procedure. The insets show the respective time evolution of $\Delta\varepsilon$ for the relaxations under investigation.

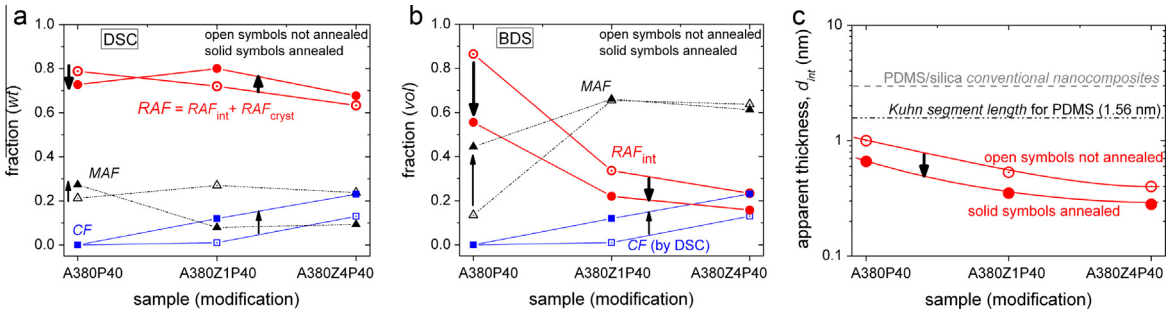

Fig. 9. Effects of surface modifications and thermal annealing (open/solid symbols) on (a, b) the various polymer fractions, i.e. rigid amorphous (*RAF*), mobile amorphous (*MAF*) and crystalline polymer (*CF*), and on (c) the apparent thickness of the interfacial layer, d_{int} (Eq. (11)), for samples of 40 wt% adsorbed PDMS. Results are shown comparatively as estimated from (a) DSC and (b, c) BDS measurements (details in text). The lines that connect the experimental data have no physical meaning and are used as guides for the eyes. The arrows mark changes imposed by thermal annealing.

Bulk-unaffected mobility of PDMS is monitored by α relaxation, characterized by an almost universal time scale in the Arrhenius diagram (Fig. 4a), as compared to different types of PDMS [9,17]. The relaxation is present in A380Z1P40 and neat PDMS. α is the only asymmetric in shape ($\beta_{HN} < 1$) relaxation recorded in the present work (Table 3), while its strength, $\Delta\varepsilon$, decreases with temperature (Fig. 4b), as expected for bulk-unconstrained segmental dynamics [42,66].

Quite standard is also the time scale of α_c relaxation (Figs. 4a and 5a), which describes the retarded dynamics of polymer chains restricted inside A-380 voids or/and between the PDMS crystals [9,17], and is recorded in all samples. $\Delta\varepsilon$ of α_c increases with temperature (Figs. 4b and 5b), as the constraints imposed by the crystals are gradually loosened [44,50]. In the case of measurements after crystallization annealing, α_c and *S* relaxations, whenever recorded, are enhanced (Fig. 7) at the expenses of bulk and interfacial polymer (α and α_{int}, respectively), without significant changes in fragility and shape parameters.

Any effects of zirconia modification on the evolution of α and α_c relaxations are again indirect, depending on the changes in X_c [9,17].

4.4. Interfacial dynamics (α_{int} relaxation)

We suggest that α_{int} monitors directly the dynamics of semi-bound polymer chains in the interfacial layer (RAF_{int}) [8,9,16,27]. Its dielectric strength in Figs. 4b and 5b is higher for unmodified A-380, for both amounts of adsorbed PDMS. The relaxation tends to become slower, weaker and less fragile (cooperative [66]) with zirconia modification (Figs. 4 and 5, Table 3). The changes recorded by BDS follow very nicely the respective changes in specific surface area, S_{BET}, in Table 1. From the methodological point of view, these results may suggest that the adsorption of gas molecules (Nitrogen in our case) on surfaces of nanometric roughness is representative also for polymer chains adsorption [17].

Another point of interest is the temperature dependence of $\Delta\varepsilon$ for α_{int} relaxation. We follow in Figs. 4b and 5b that for the strong α_{int} relaxations of A380P40 and A380P80 (i.e. unmodified samples) $\Delta\varepsilon$ increases with temperature. Simultaneously with the weakening of α_{int} relaxation with zirconia modification, $\Delta\varepsilon$ tends to decrease with temperature (Figs. 4b and 5b). This behavior resembles that of conventional nanocomposites of crosslinked PDMS [8] and natural rubber [16] filled with *in situ* generated silica particles (~5 nm in diameter), where $\Delta\varepsilon$ of α_{int} relaxation was lower than that of α and decreased with increasing temperature.

4.5. Interpretation in terms of models

In a recent study concerning interfacial phenomena in the same unmodified *core–shell* systems we have proposed that the characteristics of α_{int} relaxation are determined by PDMS chain conformations and polarizability at interfaces [17]. More specifically, according to recent studies on adsorbed polymers [6,20,21] there may exist two populations of chain segments at interfaces which can be considered responsible for the molecular mobility recorded in BDS as the interfacial α_{int} process, i.e. (a) extended tails with bulk-like density but reduced mobility and cooperativity (Scheme 1a), and (b) flattened chain segments which form the inner quite dense region due to multiple contact points with the silica surface (loops, Scheme 1a). We assume that in our *core–shell* nanocomposites, the relatively high S_{BET} values of A-380 particles are responsible for the successful adsorption of PDMS chains with a high ratio of loops/tails (Scheme 1a), due to the high number of potential particle–polymer contact points.

Additionally, for samples of respectively high/low interfacial polymer fraction (RAF_{int}) we may interpret the respective increase/decrease of $\Delta\varepsilon$ of α_{int} relaxation with temperature (Figs. 4b and 5b) as follows. According to the models described above, the loop-like conformed chains are weakly attached [20,21] on the surfaces and their concentration can increase as temperature increases, without change in interfacial polymer density, e.g. by simultaneous decrease of loops' maximum distance (height) from the adsorbing surface [21], similarly to polymers adsorbed onto solid surfaces during chemical [19] and

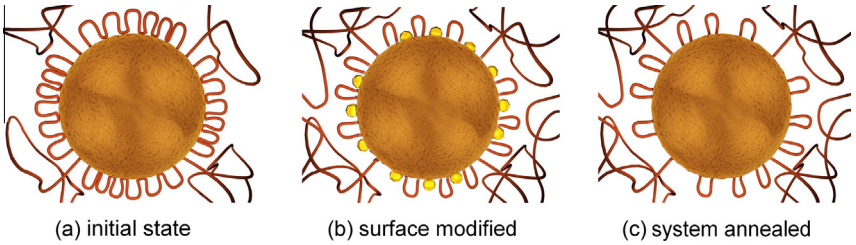

Scheme 1. Proposed 2-D schematic simplified models for describing interfacial polymer dynamics for (a) unmodified A-380 particles, (b) surface modified A-380 and (c) thermally annealed systems.

thermal [20] annealing. On the other hand, in the case of higher tail/loop ratio (Schemes 1b and c, i.e. case of lower RAF_{int} and, respectively, lower $\Delta\varepsilon$ of α_{int}) the mobility of the tails (bulk-like density) can gradually increase, drifted by the increasing of bulk-like polymer mobility. Thus, the degree of 'immobilization' and 'orientation' of the tails at the interfaces is suppressed, leading to lowering of $\Delta\varepsilon$ for α_{int} with temperature (thinner interfacial layer [8,16]).

The adequacy of the model proposed above was examined also in our recent works in similar systems of silica/PDMS by means of (a) surface modification of initially low S_{BET} silica with zirconia nanoparticles [27] and (b) thermal (crystallization) annealing [17], the results being in qualitative agreement with those obtained in the present study. It should be noted that the existence of multi-conformational segments [31] in polymer melts adsorbed on solid surfaces has been studied by computer simulations and the effects of the polymer chain length [3,32,33] and of the range of attraction of the solid surface [29,30] on interfacial polymer structure and dynamics have been predicted. Furthermore, in work in progress we follow the above model employing PDMS of different molecular weights (namely, different chain lengths) as a crucial parameter for polymer adsorption and adoption of bimodal conformations in the interfacial layer with nanooxides (silica and titania).

Finally, we recall that in previous studies on PDMS filled with *in situ* generated and finely dispersed silica (~5 nm) and titania (~30 nm) nanoparticles, the thickness of the interfacial layer, d_{int}, was ~2 nm for silica and ~4 nm for titania [8,9]. Similar values can be compatible with our results and the above models about polymer chain conformations (Scheme 1) of the bound polymer layer(s), taking into consideration that the length of *Kuhn segment* for a PDMS in melt is ~1.56 nm [72]. However, the geometrical models employed previously for the estimation of interfacial layer thickness [8,9,15] cannot not be employed here, due to the high degree of initial particles aggregation [17], the not well defined shape of aggregates (SEM images in [17]), and the significant intraparticle porosity [36]. Nevertheless, we may calculate the '*apparent*' interfacial layer thickness in our core–shell nanocomposites from the fraction of interfacial polymer, estimated above, and the specific surface area of the oxide sample before polymer adsorption, S_{BET}, determined by nitrogen adsorption–desorption measurements (Table 1). Assuming (i) constant density of PDMS in the interfacial layer and in bulk, equal to that of neat PDMS (ρ_{PDMS} = 1.62 g/m^3 [9]) and (ii) accessibility of the whole oxide surface area corresponding to S_{BET} to PDMS, we estimate the *apparent interfacial layer thickness*, d_{int}, by the following equation

$$d_{int} = \frac{volume_{interfacial,PDMS}}{surface_{interfacial}} = \frac{mass_{sample} \cdot X_{PDMS} \cdot RAF_{int}/\rho_{PDMS}}{mass_{sample} \cdot (1 - X_{PDMS}) \cdot S_{BET}} \quad (11)$$

Please note that because of assumption (ii) the calculated values represent a lower bound of the interfacial layer thickness. The results of d_{int} calculation are shown in Fig. 9c comparatively for modified (0.40–0.53 nm)/unmodified (1.00 nm) and annealed (0.28–0.66 nm)/not annealed (0.40–1.00 nm) samples. Thus, d_{int} decreases on surface modification by zirconia and on annealing. Absolute values of d_{int} in our core–shell nanocomposites (0.28–1.00 nm) are smaller than values obtained in conventional PDMS/silica nanocomposites (~2 nm) [8,9] and also smaller than the Kuhn segment length for PDMS (~1.56 nm, Fig. 9c, [72]). Please compare [15] with respect to the discussion of d_{int} in relation to *Kuhn segment length*. The relatively low absolute values can be probably understood in terms of assumption (ii) above. Results could be rationalized in future work by recording changes in density of the interfacial polymer, which has been found higher than that in bulk in previous work on polystyrene (PS) [4,21].

4.5.1. Effects of surface modification

The suppression of textural pore volume, V_p in Table 1, and of RAF_{int} (Fig. 9) with surface modification and, at the same time, of interfacial dynamics (Figs. 4 and 5) and cooperativity (Table 3), suggest strongly that, according to the model described above, the loops/tails ratio on A-380 is lower for modified samples (Scheme 1b). This assumption can be rationalized in terms of decreasing of the number of polymer–silica contact points due to the smoothening of interfacial area [36], in general. Additionally, this decrease in contact-points concentration implies an increase of the cooperativity length ξ and, thus, in the frame of Adam-Gibbs theory [73], slower and less cooperative segmental dynamics, in agreement with results for α_{int} in the present work. Similar effects were previously reported on the interfacial PDMS fraction in conventional nanocomposites, which was suppressed at the smoothed surfaces of titania (relatively low surface area, S_{BET}), as compared to the rather diffused surfaces of silica (relatively high surface area) [9] and Ref. 23 therein. Finally, we have recently showed

that similar zirconia modification on low specific surface area fumed silica (58 m^2/g) [27] resulted in slightly increased S_{BET} and in faster and more cooperative interfacial relaxation, these effects suggesting an increase of PDMS–particle contact points, in qualitative agreement with effects obtained here with S_{BET} and α_{int} of A-380 based nanocomposites.

4.5.2. Effects of thermal (crystallization) annealing

In the nanocomposites of both modified and unmodified A-380 which have suffered thermal annealing (a) α_{int} relaxation has immigrated toward higher temperatures/lower frequencies (Fig. 7a) and (b) $\Delta\varepsilon$ of α_{int} has been suppressed (Figs. 7b and 8b). The changes are less pronounced for the samples of modified A-380, where α_{int} was already weaker and slower as compared to the unmodified A-380. Thus, the effects imposed by annealing seem to be in the same direction with those of surface modification, as far as interfacial dynamics and fraction is concerned. The changes can be interpreted, again, in terms of reorganization of chain distribution in the interfacial layer. More specifically, some of the chains could be detached during annealing, resulting in the restriction of concentration and mobility of the loops (Scheme 1c), which are probably more loosely attached onto the surfaces as compared to the tails [21]. Additional support to this explanation is given by (a) DSC in Table 2 (Fig. 9a) for A380P40, for which we follow increasing of $\Delta C_{p,n}$ (*MAF*) after annealing, without simultaneous increase in X_c (*CF*), and (b) BDS in Fig. 7 where we observed an increase of *S* relaxation, assigned to increase of the concentration of free surface hydroxyls. Similar results were reported recently for core–shell systems based on fumed silicas and PDMS, same as in the present work [17]. Other models proposed for explaining the effects of annealing in these and similar systems involve the diffusion of free volume holes at the interfaces between polymer and nanoparticles [74] or redistribution of interfacial free polymer volume [75], and, also, possible changes in interfacial polymer density [4].

5. Conclusions

Effects of surface modification and subsequent thermal treatment on molecular dynamics in silica/PDMS nanocomposites of *core–shell* type were studied in this work. The strong hydrogen bonding developed between the surface hydroxyls of silica and the oxygens of the backbone of PDMS resulted to successive adsorption of the polymer, in particular to the formation of an interfacial polymer layer on the surfaces of the particles in the silica aggregates. The amount of interfacial polymer was estimated by both calorimetric and dielectric methods to employ quite high fraction of the whole polymer (up to 90% at the low polymer loading of 40 wt% PDMS). This amount decreased for high polymer loadings, as expected. The interaction between particles and polymer was suppressed after the grafting of zirconia particles onto the surfaces of silica, by suppression of the surface available for polymer–filler interaction. The changes were reflected both in the thermal transitions (e.g. enhanced crystallization and glass transition) and the evolution of segmental dynamics, as recorded through specific dielectric relaxations.

BDS was found able to record the segmental dynamics of PDMS in the polymer–particle interfacial layer (α_{int} relaxation). Surface modification and thermal annealing were found to impose similar effects on interfacial dynamics, both resulting in a reduction of the number of polymer–particle contact points on the surfaces of silica. As a result, interfacial polymer fraction, dynamics and cooperativity were suppressed. Furthermore, changes in specific characteristics of the interfacial relaxation could be interpreted in terms of bimodal conformations (tail- and loop-like) of the adsorbed PDMS chains at interfaces, the concentration of which seems to decrease, especially that of loops, with the reduction of the number of contact points accessible to polymer on the modified surfaces. By employing a combination of DSC and BDS results we were able to monitor the additional lowering of interfacial polymer density after thermal annealing (related also with enhanced crystallization) of the samples. In agreement to recently presented findings [17,27], this result suggests that the loop-like interfacial polymer conformations are more weakly attached than tail-like chains [21]. In addition, the results obtained in the present work enabled to reconsider previous results on conventional PDMS/silica and PDMS/titania nanocomposites [8,9], now from a different perspective. Thus, we concluded that the reported shift of interfacial dynamics to lower frequencies/higher temperatures in the titania as compared to the silica nanocomposites may not originate exclusively from the higher strength of PDMS–titania hydrogen bonding (type of particle) [9] or from the size of oxide particles [15], but determined also by the concentration of contact points on the surfaces of aggregates/nanoparticles available for polymer adsorption, the latter being quantitatively well described by the surface roughness (S_{BET}) of the aggregates/particles [17]. With respect to dynamics, conformations and density of polymer in the interfacial layer, new challenging questions arose from the present study and could be further followed, in future work, by properly designed experiments on PDMS adsorbed at various amounts on fumed silica and silica-like (e.g. titania, zirconia) particles of a broad range of specific surface area (surface roughness).

Acknowledgements

The authors would like to thank Prof. Vladimir M. Gun'ko from the Institute of Surface Chemistry of the National Academy of Sciences of Ukraine, for providing the materials, Dr. Daniel Fragiadakis for providing a sophisticated analysis software (http://grafitylabs.com/), Mr. Konstantinos Kyriakos and Mr. Ioannis Vangelidis for contributing to experiments, and the graphic designer Mr. Dimitrios Klonos (http://dimitrisklonos.blogspot.gr/) for the illustrations.

This research has been co-financed by the European Union (European Social Fund – ESF) and Greek national funds through the Operational Program "Education and Lifelong Learning" of the National Strategic Reference Framework

(NSRF) – Research Funding Programs: Heracleitus II. Investing in knowledge society through the European Social Fund (P.K. and P.P.) and Research Funding Program: Aristeia (A.K. and P.P.). This research was partially supported by FP7 – PIRSES-GA-2013-612484 NANOBIOMAT.

Appendix A. Supplementary material

Supplementary data associated with this article can be found, in the online version, at http://dx.doi.org/10.1016/j.eurpolymj.2015.07.038.

References

[1] D.R. Paul, L.M. Robenson, Polymer nanotechnology: nanocomposites, Polymer 49 (2008) 3187–3204, http://dx.doi.org/10.1016/j.polymer.2008.04.017.
[2] L. Bokobza, J.P. Chauvin, Reinforcement of natural rubber: use of in situ generated silicas and nanofibres of sepiolite, Polymer 46 (2005) 4144–4151, http://dx.doi.org/10.1016/j.polymer.2005.02.048.
[3] V.A. Harmandaris, K.C. Daoulas, V.G. Mavrantzas, Molecular dynamics simulation of a polymer melt/solid interface: local dynamics and chain mobility in a thin film of polyethylene melt adsorbed on graphite, Macromolecules 38 (2005) 5796–5809, http://dx.doi.org/10.1021/ma050177j.
[4] G.G. Vogiatzis, E. Voyiatzis, D.N. Theodorou, Monte Carlo simulations of a coarse grained model for an athermal all-polystyrene nanocomposite system, Eur. Polym. J. 47 (2011) 699–712, http://dx.doi.org/10.1016/j.eurpolymj.2010.09.017.
[5] H. Eslami, M. Rahimi, F. Müller-Plathe, Molecular dynamics simulation of a silica nanoparticle in oligomeric poly(methyl methacrylate): a model system for studying the interphase thickness in a polymer-nanocomposite via different properties, Macromolecules 46 (2013) 8680–8692, http://dx.doi.org/10.1021/ma401443v.
[6] G. Kritkos, A.F. Terzis, Variable density self consistent field study on bounded polymer layer around spherical nanoparticles, Eur. Polym. J. 49 (2013) 613–629, http://dx.doi.org/10.1016/j.eurpolymj.2012.09.008.
[7] K. Johnston, V. Harmandaris, Hierarchical simulations of hybrid polymer-solid materials, Soft Matter 9 (2013) 6696–6710, http://dx.doi.org/10.1039/C3SM50330E.
[8] D. Fragiadakis, P. Pissis, Glass transition and segmental dynamics in poly(dimethylsiloxane)/silica nanocomposites studied by various techniques, J. Non-Cryst. Solids 353 (2007) 4344–4352, http://dx.doi.org/10.1016/j.jnoncrysol.2007.05.183.
[9] P. Klonos, A. Panagopoulou, L. Bokobza, A. Kyritsis, V. Peoglos, P. Pissis, Comparative studies on effects of silica and titania nanoparticles on crystallization and complex segmental dynamics in poly(dimethylsiloxane), Polymer 51 (2010) 5490–5499, http://dx.doi.org/10.1016/j.polymer.2010.09.054.
[10] M. Füllbrandt, P.J. Purohit, A. Schönhals, Combined FTIR and dielectric investigation of poly(vinyl acetate) adsorbed on silica particles, Macromolecules 46 (2013) 4626–4632, http://dx.doi.org/10.1021/ma400461p.
[11] A.P. Holt, P.J. Griffin, V. Bocharova, A.L. Agapov, A.E. Imel, M.D. Dadmun, J.R. Sangoro, A.P. Sokolov, Dynamics at the polymer/nanoparticle interface in poly(2-vinylpyridine)/silica nanocomposites, Macromolecules 47 (2014) 1837–1843, http://dx.doi.org/10.1021/ma5000317.
[12] M.V. Galaburda, P. Klonos, V.M. Gun'ko, V.M. Bogatyrov, M.V. Borysenko, P. Pissis, Dielectric properties and thermal destruction of poly(dimethylsiloxane)/Fe_2O_3/SiO_2 nanocomposites, Appl. Surf. Sci. 305 (2014) 67–76, http://dx.doi.org/10.1016/j.apsusc.2014.02.162.
[13] I. Sulym, P. Klonos, M. Borysenko, P. Pissis, V.M. Gun'ko, Dielectric and thermal studies of segmental dynamics in silica/PDMS and silica/titania/PDMS nanocomposites, J. Appl. Polym. Sci. 131 (2014) 41154, http://dx.doi.org/10.1002/app.4115.
[14] P. Akcora, H. Liu, S.K. Kumar, J. Moll, Y. Ki, B.C. Benicewicz, L.S. Schadler, D. Acehan, A.Z. Panagiotopoulos, V. Pryamitsyn, V. Ganesan, J. Ilavsky, R. Thiyagarajan, R.H. Colby, J.F. Douglas, Anisotropic self-assembly of spherical polymer-grafted nanoparticles, Nat. Mater. 8 (2009) 354–359, http://dx.doi.org/10.1038/nmat2404.
[15] S. Gong, Q. Chen, J.F. Moll, S.K. Kumar, R.H. Colby, Segmental dynamics of polymer melts with spherical nanoparticles, ACS Macro Lett. 3 (2014) 773–777, http://dx.doi.org/10.1021/mz500252f.
[16] D. Fragiadakis, L. Bokobza, P. Pissis, Dynamics near the filler surface in natural rubber-silica nanocomposites, Polymer 52 (2011) 3175–3182, http://dx.doi.org/10.1016/j.polymer.2011.04.045.
[17] P. Klonos, I.Y. Sulym, M.V. Borysenko, V.M. Gun'ko, S. Kripotou, A. Kyritsis, P. Pissis, Interfacial interactions and complex segmental dynamics in systems based on silica-polydimethylsiloxane core–shell nanoparticles: dielectric and thermal study, Polymer 58 (2015) 9–21, http://dx.doi.org/10.1016/j.polymer.2014.12.03.
[18] P. Klonos, Ch. Pandis, S. Kripotou, A. Kyritsis, P. Pissis, Interfacial effects in polymer nanocomposites studied by dielectric and thermal techniques, IEEE Trans. Diel. Electr. Insul. 19 (2012) 4, http://dx.doi.org/10.1109/TDEI.2012.6260002.
[19] L.T. Lee, O. Guiselin, A. Lapp, B. Farnoux, J. Penfold, Direct measurements of polymer depletion layers by neutron reflectivity, Phys. Rev. Lett. 67 (1991) 2838–2841, http://dx.doi.org/10.1103/PhysRevLett. 67.2838.
[20] C. Rotella, S. Napolitano, S. Vandendriessche, V.K. Valev, T. Verbiest, M. Larkowska, S. Kucharski, M. Wübbenhorst, Adsorption kinetics of ultrathin polymer films in the melt probed by dielectric spectroscopy and second-harmonic generation, Langmuir 27 (2011) 13533–13538, http://dx.doi.org/10.1021/la2027779.
[21] P. Gin, N. Jiang, C. Liang, T. Taniguchi, B. Akgun, S.K. Satija, M.K. Endoh, T. Koga, Revealed architectures of adsorbed polymer chains at solid-polymer melt interfaces, Phys. Rev. Lett. 109 (2012) 265501, http://dx.doi.org/10.1103/PhysRevLett. 109.265501.
[22] S. Capponi, S. Napolitano, M. Wübbenhorst, Supercooled liquids with enhanced orientational order, Nat. Commun. 3 (2012) 1233, http://dx.doi.org/10.1038/ncomms2228.
[23] B. Vanroy, W. Wübbenhorst, S. Napolitano, Crystallization of thin polymer layers confined between two adsorbing walls, ACS Macro Lett. 2 (2013) 168–172, http://dx.doi.org/10.1021/mz300641x.
[24] S. Napolitano, C. Rotella, M. Wübbenhorst, Can thickness and interfacial interactions univocally determine the behavior of polymers confined at the nanoscale?, ACS Macro Lett 1 (2012) 1189–1193, http://dx.doi.org/10.1021/mz300432d.
[25] V. Bershtein, V. Gun'ko, L. Egorova, N. Guzenko, E. Pakhlov, V. Ryzhov, V. Zarko, Well-defined silica core-poly(vinyl pyrrolidone) shell nanoparticles: Interactions and multi-modal glass transition dynamics at interfaces, Polymer 50 (2009) 860–871, http://dx.doi.org/10.1016/j.polymer.2008.12.02.
[26] Y.L. Liu, E. Chen, Polymer crystallization of ultrathin films on solid substrates, Coord. Chem. Rev. 254 (2010) 1011–1037, http://dx.doi.org/10.1016/j.ccr.2010.02.017.
[27] P. Klonos, I.Y. Sulym, K. Kyriakos, I. Vangelidis, S. Zidropoulos, D. Sternik, M.V. Borysenko, A. Kyritsis, A. Deryło-Marczewska, V.M. Gun'ko, P. Pissis, Interfacial phenomena in core–shell nanocomposites of PDMS adsorbed onto low specific surface area fumed silica nanooxides: effects of surface modification, Polymer 68 (2015) 158–167, http://dx.doi.org/10.1016/j.polymer.2015.05.01.
[28] P. Klonos, P. Pissis, V.M. Gun'ko, A. Kyritsis, N.V. Guzenko, E.M. Pakhlov, V.I. Zarko, W. Janusz, J. Skubiszewska-Zięba, R. Leboda, Interaction of poly(ethylene glycol) with fumed silica and alumina/silica/titania, Colloid. Surf. A: Physicochem. Eng. Asp. 360 (2010) 220–231, http://dx.doi.org/10.1016/j.colsurfa.2010.03.00.
[29] K.F. Mansfield, D.N. Theodorou, Interfacial structure and dynamics of macromolecular liquids: a Monte Carlo simulation approach, Macromolecules 22 (1989) 3143–3152, http://dx.doi.org/10.1021/ma00197a042.

[30] O. Borodin, G.D. Smith, R. Bandyopadhyaya, O. Byutner, Molecular dynamics study of the influence of solid interfaces on poly(ethylene oxide) structure and dynamics, Macromolecules 36 (2003) 7873–7883, http://dx.doi.org/10.1021/ma0346005.
[31] J.M.H.M. Scheutjens, G.J. Fleer, Statistical theory of the adsorption of interacting chain molecules. 1. Partition function, segment density distribution, and adsorption isotherms, J. Phys. Chem. 83 (1979) 1619–1635, http://dx.doi.org/10.1021/j100475a012.
[32] I.A. Bitsanis, G. Brinke, A lattice Monte Carlo study of long chain conformations at solid–polymer melt interfaces, J. Chem. Phys. 99 (1993) 3100, http://dx.doi.org/10.1063/1.46516.
[33] K.C. Daoulas, V.A. Harmandaris, V.G. Mavrantzas, Detailed atomistic simulation of a polymer melt/solid interface: structure, density, and conformation of a thin film of polyethylene melt adsorbed on graphite, Macromolecules 38 (2005) 5780–5795, http://dx.doi.org/10.1021/ma050176r.
[34] K. Johnston, V. Harmandaris, Hierarchical multiscale modeling of polymer–solid interfaces: atomistic to coarse-grained description and structural and conformational properties of polystyrene-gold systems, Macromolecules 46 (2013) 5741–5750, http://dx.doi.org/10.1021/ma400357r.
[35] R.L. Jones, S.K. Kumar, D.L. Ho, R.M. Briber, T.P. Russell, Chain conformation in ultrathin polymer films, Nature 400 (1999) 146–149, http://dx.doi.org/10.1038/22080.
[36] I.Y. Sulim, M.V. Borysenko, O.M. Korduban, V.M. Gun'ko, Influence of silica matrix morphology on characteristics of grafted nanozirconia, Appl. Surf. Sci. 255 (2009) 7818–7824, http://dx.doi.org/10.1016/j.apsusc.2009.04.185.
[37] V.M. Gun'ko, V.V. Turov, A.A. Turova, T.V. Krupska, P. Pissis, R. Leboda, Skubiszewska-Zieba, Interactions of poly(dimethylsiloxane) with nanosilica and silica gel upon cooling–heating, J. Colloids Interf. Sci. 426 (2014) 48–55, http://dx.doi.org/10.1016/j.jcis.2014.03.05.
[38] M.F. Morks, A. Kobayashi, Fabrication and characterization of plasma-sprayed HA/SiO_2coatings for biomedical application, J. Mech. Behav. Biomed. Mater. 1 (2008) 165–171, http://dx.doi.org/10.1016/j.jmbbm.2007.04.003.
[39] C. Stamatopoulou, P. Klonos, S. Koutsoumpis, V.M. Gun'ko, P. Pissis, L. Karabanova, Hydrophilic nanocomposites based on polyurethane/poly(2-hydroxyethyl methacrylate) semi-IPNs and modified/unmodified nanosilica for biomedical applications, J. Appl. Polym. Sci. B: Polym. Phys. 52 (2014) 397–408, http://dx.doi.org/10.1002/polb.2342.
[40] P. Klonos, A. Panagopoulou, A. Kyritsis, L. Bokobza, P. Pissis, Dielectric studies of segmental dynamics in poly(dimethylsiloxane)/titania nanocomposites, J. Non-Cryst. Solids 357 (2011) 610–614, http://dx.doi.org/10.1016/j.jnoncrysol.2010.06.058.
[41] M. Aranguren, Crystallization of polydimethylsiloxane: effect of silica filler and curing, Polymer 39 (1998) 4897–4903, http://dx.doi.org/10.1016/S0032-3861(97)10252-X.
[42] F. Kremer, A. Schönhals (Eds.), Broadband Dielectric Spectroscopy, Springer, Berlin, 2002.
[43] A. Wurm, R. Soliman, C. Schick, Early stages of polymer crystallization – a dielectric study, Polymer 44 (2003) 7467–7476, http://dx.doi.org/10.1016/j.polymer.2003.09.028.
[44] R. Lund, A. Alegría, L. Goitandia, J. Colmenero, M.A. Gonzaalez, P. Lindner, Dynamical and structural aspects of the cold crystallization of poly(dimethylsiloxane) (PDMS), Macromolecules 41 (2008) 1364–1376, http://dx.doi.org/10.1021/ma702055b.
[45] C. Alvarez, I. Šics, A. Nogales, Z. Denchev, S.S. Funari, T.A. Ezquerra, Structure–dynamics relationship in crystallizing poly(ethylene terephthalate) as revealed by time-resolved X-ray and dielectric methods, Polymer 45 (2004) 3953–3959, http://dx.doi.org/10.1016/j.polymer.2003.09.069.
[46] G.Z. Papageorgiou, Z. Terzopoulou, D. Bikiaris, K.S. Triantafyllidis, E. Diamanti, D. Gournis, P. Klonos, E. Giannoulidis, P. Pissis, Evaluation of the formed interface in biodegradable poly(l-lactic acid)/graphene oxide nanocomposites and the effect of nanofillers on mechanical and thermal properties, Thermochim. Acta 597 (2014) 48–57, http://dx.doi.org/10.1016/j.tca.2014.10.007.
[47] S. Havriliak, S. Negami, A complex plane representation of dielectric and mechanical relaxation processes in some polymers, Polymer 8 (1967) 161–210, http://dx.doi.org/10.1016/0032-3861(67)90021-3.
[48] V.M. Gun'ko, V.V. Turov, Nuclear Magnetic Resonance Studies of Interfacial Phenomena, CRC Press, Boca Raton, 2013.
[49] B. Wunderlich, The ATHAS database on heat capacities of polymers, Pure Appl. Chem. 67 (1995) 1019–1026, http://dx.doi.org/10.1351/pac199567061019. http://athas.prz.edu.pl/Default.aspx?op=db.
[50] U.W. Gedde, Polymer Physics, Chapman & Hall, London, 1995.
[51] E. Zhuravlev, A. Wurm, P. Pötschke, R. Androsch, J.W.P. Schmelzer, C. Schick, Kinetics of nucleation and crystallization of poly(ε-caprolactone) – Multiwalled carbon nanotube composites, Eur. Polym. J. 52 (2014) 1–11, http://dx.doi.org/10.1016/j.eurpolymj.2013.12.015.
[52] J. Dobbertin, A. Hensel, C. Schick, Dielectric spectroscopy and calorimetry in the glass transition region of semicrystalline poly(ethylene terephthalate), J. Thermal Anal. Calorim. 47 (1996) 1027–1040, http://dx.doi.org/10.1007/BF01979446.
[53] A. Wurm, M. Ismail, B. Kretzschmar, D. Pospiech, C. Schick, Retarded crystallization in polyamide/layered silicates nanocomposites caused by an immobilized interphase, Macromolecules 43 (2010) 1480–1487, http://dx.doi.org/10.1021/ma902175r.
[54] H. Xu, P. Cebe, Heat capacity study of isotactic polystyrene: dual reversible crystal melting and relaxation of rigid amorphous fraction, Macromolecules 37 (2004) 2797–2806, http://dx.doi.org/10.1021/ma035961n.
[55] P.J. Purohit, D. Wang, A. Wurm, C. Schick, A. Schönhals, Comparison of thermal and dielectric spectroscopy for nanocomposites based on polypropylene and Layered Double Hydroxide – Proof of interfaces, Eur. Polym. J. 55 (2014) 48–56, http://dx.doi.org/10.1016/j.eurpolymj.2014.03.005.
[56] P. Brauenlich, Thermally Stimulated Relaxation in Solids, Springer, Berlin, 1979.
[57] L. Bokobza, A.L. Diop, Reinforcement of poly(dimethylsiloxane) by sol–gel in situ generated silica and titania particles, Express Polym. Lett. 4 (2010) 355–363, http://dx.doi.org/10.3144/expresspolymlett.2010.45.
[58] V.M. Gun'ko, V.V. Turov, V.M. Bogatyrev, V.I. Zarko, R. Leboda, E.V. Goncharuk, A.A. Novza, A.V. Turov, A.A. Chuiko, Unusual properties of water at hydrophilic/hydrophobic interfaces, Adv. Colloid Interf. Sci. 118 (2005) 125–172, http://dx.doi.org/10.1016/j.cis.2005.07.00.
[59] H. Vogel, The law of the relation between the viscosity of liquids and the temperature, Phys. Z 22 (1921) 645–646;
G.S. Fulcher, Analysis of recent measurements of viscosity of glasses, J. Am. Ceram. Soc. 8 (1925) 339–355, http://dx.doi.org/10.1111/j.1151-2916.1925.tb16731.x;
G. Tammann, W. Hesse, Die Abhängigkeit der Viscosität von der Temperatur bie unterkühlten Flüssigkeiten, Z. Anorg. Allg. Chem. 156 (1926) 245–257, http://dx.doi.org/10.1002/zaac.19261560121.
[60] R. Richert, C.A. Angell, Dynamics of glass-forming liquids. V. On the link between molecular dynamics and configurational entropy, J. Chem. Phys. 108 (21) (1998) 9016–9026, http://dx.doi.org/10.1063/1.476348.
[61] R. Boehmer, K. Ngai, C.A. Angell, D.J. Plazek, Nonexponential relaxations in strong and fragile glass formers, J. Chem. Phys. 99 (1993) 4201–4209, http://dx.doi.org/10.1063/1.466117.
[62] Y. Suzuki, H. Duran, M. Steinhart, H.J. Butt, G. Floudas, Homogeneous crystallization and local dynamics of poly(ethylene oxide) (PEO) confined to nanoporous alumina, Soft Matter 9 (2013) 2621–2628, http://dx.doi.org/10.1039/c2sm27618f.
[63] J.J. Fontanella, M.C. Wintersgill, C.A. Edmondson, J.F. Lomax, Water-associated dielectric relaxation in oxide nanoparticles, J. Phys. D: Appl. Phys. 42 (2009) 042003, http://dx.doi.org/10.1088/0022-3727/42/4/04200;
J.J. Fontanella, J.T. Bendler, D.E. Schuele, C.A. Edmondson, J.F. Lomax, Effect of pressure on the water relaxation in glassy polyetherimide, J. Non-Cryst. Solids 353 (2007) 4528–4532, http://dx.doi.org/10.1016/j.jnoncrysol.2007.01.08.
[64] P. Klonos, S. Kaprinis, V.I. Zarko, V. Peoglos, E.M. Pakhlov, P. Pissis, V.M. Gun'ko, Thermal and dielectric studies of PEG/C/AST nanocomposites, J. Appl. Polym. Sci. 128 (2013) 1601–1615, http://dx.doi.org/10.1002/app.3795.
[65] A. Schönhals, H. Goering, Ch. Schick, B. Frick, R. Zorn, Glassy dynamics of polymers confined to nanoporous glasses revealed by relaxational and scattering experiments, Eur. Phys. J. E12 (2003) 173–178, http://dx.doi.org/10.1140/epje/i2003-10036-4.
[66] E. Donth, The glass transition: relaxation dynamics in liquids and disordered materials, Springer Series in Materials Science, vol. 48, Springer, Berlin, 2001.
[67] K.L. Ngai, Relation between some secondary relaxations and the α relaxations in glass-forming materials according to the coupling model, J. Chem. Phys. 109 (1998) 6982–6994, http://dx.doi.org/10.1063/1.477334.

[68] G.P. Johari, M. Goldstein, Molecular mobility in simple glasses, J. Phys. Chem. 74 (1970) 2034–2035, http://dx.doi.org/10.1021/j100704a038.
[69] J. Khan, S.E. Harton, P. Ackora, B.C. Benicewicz, S.K. Kumar, Polymer crystallization in nanocomposites: spatial reorganization of nanoparticles, Macromolecules 42 (2009) 5741–5744, http://dx.doi.org/10.1021/ma900794t.
[70] P.R. Sundararajan, Crystalline morphology of poly(dimethylsiloxane), Polymer 43 (2002) 1691–1693, http://dx.doi.org/10.1016/S0032-3861(01)00743-1.
[71] M. Krutyeva, A. Wischnewski, L. Wilner, J. Maiz, C. Mijangos, A. Arbe, J. Colmenero, A. Radulescu, O. Holderer, M. Ohl, D. Richter, Effect of nanoconfinement on polymer dynamics: surface layers and interphases, Phys. Rev. Lett. 110 (2013) 108303, http://dx.doi.org/10.1103/PhysRevLett.110.108303.
[72] N. Gilra, C. Cohen, R.M. Briber, B.J. Bauer, R.C. Hedden, A.Z. Panagiotopoulos, A SANS study of the conformational behaviour of linear chains in compressed and uncompressed end-linked elastomers, Macromolecules 34 (2001) 7773–7782, http://dx.doi.org/10.1021/ma010018+.
[73] G. Adam, J.H. Gibbs, On the temperature dependence of cooperative relaxation properties in glass-forming liquids, J. Chem. Phys. 43 (1965) 139–146, http://dx.doi.org/10.1063/1.1696442.
[74] F. Barroso-Bujans, P. Palomino, S. Cerveny, F. Fernandez-Alonso, S. Rudić, A. Alegría, J. Colmenero, E. Enciso, Confinement of poly(ethylene oxide) in the nanometer-scale pores of resins and carbon nanoparticles, Soft Matter 9 (2013) 10690–10695, http://dx.doi.org/10.1039/c3sm51563j.
[75] S. Napolitano, A. Pilleri, P. Rolla, W. Wübbenhorst, Unusual deviations from bulk behavior in ultrathin films of poly(tert-butylstyrene): can dead layers induce a reduction of T_g?, ACS Nano 4 (2010) 841–848, http://dxdoi.org/10.1021/nn9014517.